Structure and dynamics of water in nanoscopic spheres and tubes

van der Loop, T.H.; Ottosson, N.; Lotze, S.; Kentzinger, E.; Vad, T.; Sager, W.F.C.; Bakker, H.J.; Woutersen, S.

DOI
10.1063/1.4898380

Publication date
2014

Document Version
Final published version

Published in
Journal of Chemical Physics

Structure and dynamics of water in nanoscopic spheres and tubes

Tibert H. van der Loop,[1] Niklas Ottosson,[2] Stephan Lotze,[2] Emmanuel Kentzinger,[3] Thomas Vad,[4] Wiebke F. C. Sager,[5,a)] Huib J. Bakker,[2,b)] and Sander Woutersen[1,c)]
[1]*Van 't Hoff Institute for Molecular Sciences, University of Amsterdam, Science Park 904, 1098 XH Amsterdam, Netherlands*
[2]*FOM Institute for Atomic and Molecular Physics, Science Park 104, 1098 XG Amsterdam, The Netherlands*
[3]*Jülich Centre for Neutron Science, JARA-FIT and Peter Grünberg Institute, Forschungszentrum Jülich, 52425 Jülich, Germany*
[4]*Institut für Textiltechnik, RWTH Aachen University, Otto-Blumenthal-Str. 1, 52074 Aachen, Germany*
[5]*Ernst Ruska-Centre for Microscopy and Spectroscopy with Electrons and Peter Grünberg Institute, Forschungszentrum Jülich, 52425 Jülich, Germany*

(Received 20 August 2014; accepted 6 October 2014; published online 3 November 2014; publisher error corrected 12 November 2014)

We study the reorientation dynamics of liquid water confined in nanometer-sized reverse micelles of spherical and cylindrical shape. The size and shape of the micelles are characterized in detail using small-angle x-ray scattering, and the reorientation dynamics of the water within the micelles is investigated using GHz dielectric relaxation spectroscopy and polarization-resolved infrared pump-probe spectroscopy on the OD-stretch mode of dilute HDO:H_2O mixtures. We find that the GHz dielectric response of both the spherical and cylindrical reverse micelles can be well described as a sum of contributions from the surfactant, the water at the inner surface of the reversed micelles, and the water in the core of the micelles. The Debye relaxation time of the core water increases from the bulk value τ_{H_2O} of 8.2 ± 0.1 ps for the largest reverse micelles with a radius of 3.2 nm to 16.0 ± 0.4 ps for the smallest micelles with a radius of 0.7 nm. For the nano-spheres the dielectric response of the water is approximately ∼6 times smaller than expected from the water volume fraction and the bulk dielectric relaxation of water. We find that the dielectric response of nano-spheres is more attenuated than that of nano-tubes of identical composition (water-surfactant ratio), whereas the reorientation dynamics of the water hydroxyl groups is identical for the two geometries. We attribute the attenuation of the dielectric response compared to bulk water to a local anti-parallel ordering of the molecular dipole moments. The difference in attenuation between nano-spheres and nano-cylinders indicates that the anti-parallel ordering of the water dipoles is more pronounced upon spherical than upon cylindrical nanoconfinement. © *2014 AIP Publishing LLC*. [http://dx.doi.org/10.1063/1.4898380]

I. INTRODUCTION

Since water in living systems is often enclosed in very small volumes,[1,2] the effect of confinement to nanoscopic volumes on the structure and dynamics of water has been actively investigated over the last decade.[3–15] The properties of water in nanoconfinement have been studied with model systems like reverse micelles (water-in-oil microemulsions)[3–11] and nanoporous materials.[12–15] Reverse micelles in particular have proven to be convenient model systems because of the ease of sample preparation and the possibility of controlling the water-pool size. In addition, the chemical nature of the interface of the reverse micelle can be conveniently modified using cationic, anionic, or nonionic surfactants.

It has been suggested that the dynamics of water in a nanoscopic volume does not only depend on the size, but also on the shape of the volume. In particular, it has been predicted that one-dimensionally (cylindrically or tubular) confined water can exhibit an unusually high water mobility and allows for extremely fast ion diffusion.[16–18] Cylindrical nanoconfinement is relevant for charge transportation through the water channels of fuel cell membranes,[19] and for transport of protons and other ions through membrane-protein channels. However, to date, a systematic investigation of the effect of shape on the dynamics of nanoconfined water is lacking. Studies on reverse micelles have focused mainly on the effect of size in the case of spherical confinement,[3–11] and investigations on nanoporous materials are restricted to cylindrical geometries (channels).[12–15,20–23]

Reverse micelles can adopt spherical or cylindrical shapes, depending on the combination of apolar solvent and surfactant.[24–28] Hence, reverse micelles are excellent systems to investigate the effect of the shape of nanoconfined water volume on its dynamics. In a recent combined time-resolved fluorescence and THz time-domain spectroscopic study, no significant effect of the shape of the reverse micelle on the water dynamics was observed, but since in that study the geometry and the size of the water volume were changed simultaneously, it was difficult to isolate the influence of the shape.[29]

Here, we investigate and compare the structure and reorientation dynamics of water confined in spherical and

a)Electronic mail: w.sager@fz-juelich.de
b)Electronic mail: h.bakker@amolf.nl
c)Electronic mail: s.woutersen@uva.nl

tubular reverse micelles prepared with the non-ionic surfactant Igepal and *n*-hexane or cyclohexane as apolar solvent. We will use small-angle x-ray scattering SAXS to determine the shape and the size distribution of the micelles, and GHz dielectric relaxation spectroscopy and mid-IR vibrational pump-probe spectroscopy to investigate the influence of these parameters on the orientational dynamics of the confined water.

II. MATERIALS AND METHODS

A. Sample preparation

The composition of the reverse-micelle samples is characterized by the water to surfactant molar ratio

$$w_0 = [H_2O]/[\text{surfactant}]$$

and the surfactant mass fraction

$$c_s = \frac{m_{\text{surfactant}}}{m_{\text{oil}} + m_{\text{surfactant}}}, \quad (1)$$

where $m_{\text{surfactant}}$ and m_{oil} are the masses of the surfactant and the apolar solvent (oil), respectively. Spherical reverse-micelle samples were prepared by dissolving Igepal CO-520 (pentaoxyethylene nonylphenylether, average molar mass 441) in cyclohexane (>99.9% HPLC grade), and subsequently adding Milli-Q (18.2 MΩ cm) water to obtain the desired w_0. All samples were shaken and sonicated before the measurements. All chemicals were purchased from Sigma-Aldrich.

For the size-dependence measurements, we prepared spherical micelle samples with $w_0 = 0, 3, 5, 8$ for $c_s = 0.33$, and with $w_0 = 0, 10, 15, 20$ for $c_s = 0.28$. A larger c_s (and hence larger micelle concentration) was used for the smaller reverse micelles in order to obtain a sufficiently strong dielectric response. Cylindrical reverse micelles were prepared with *n*-hexane (>99.9% HPLC grade) as the oil phase. To study the effect of shape on the water dynamics, we prepared both cylindrical and spherical micelles with $w_0 = 5$. Using the same value of w_0 implies that the water content is the same for the two micelle shapes. For the cylindrical micelles, we used a surfactant fraction of $c_s = 0.37$ and for the spherical micelles we used $c_s = 0.33$. For the samples with the largest micelles, full equilibration took several hours, whereas the smallest reverse micelles equilibrated within minutes. After equilibration, all samples were optically clear and stable. The cylindrical micelles exhibit Rayleigh scattering in the visible.

B. Small-angle x-ray scattering

SAXS measurements were performed at the high brilliance laboratory Gallium Anode Low Angle X-ray Instrument GALAXI at the Jülich research center (Germany) equipped with a BRUKER AXS MetalJet x-ray source. The diffractometer is based on the former JUSIFA instrument installed at the DORIS storage ring at HASYLAB (Deutsches Elektronen Synchotron DESY, Hamburg, Germany). The reverse micellar samples were filled in quartz capillaries with an inner diameter of 1.5 mm and measured at room temperature ($T = 298$ K). The data were recorded with a 1 M Pilatus detector (DECTRIS) at a sample-to-detector distance of 1.7 m and a wavelength of 0.134 nm covering a range of momentum transfer of $0.06 \leq q \leq 4$ nm^{-1} ($q = 4\pi\sin(\theta)/\lambda$ is the modulus of the scattering vector, 2θ is the scattering angle, and λ is the wavelength). The collected data were radially averaged and normalized to the intensity of the transmitted beam. Solvent scattering was subtracted prior to data analysis. All samples were made at the same surfactant in oil concentrations c_s as used for the dielectric and spectroscopic experiments. The SAXS data for spherical reverse micelles were fitted by a model function based on Vrij's analytical solution for a multi-component system of hard spheres.[30–32] The characteristics of long semi-flexible worm-like micelles were analyzed using the Kholodenko model.[33] To obtain structural information on interconnected cylindrical networks, the Teubner-Strey Model has been applied to fit the microemulsion peak occurring at high volume fraction, that is typical for bicontinuous microemulsions or sponge phases.[34] The fits of the model curves to the observed SAXS data were performed with a nonlinear Levenberg-Marquardt least-squares algorithm.[35]

C. GHz dielectric relaxation spectroscopy (DRS)

We performed DRS measurements of reverse micelles in the frequency range between 100 MHz and 30 GHz with a vector network analyzer (VNA, Rhode-Schwartz model ZVA67). With this system we perform reflectometry measurements using two different home-built sample cells, thus directly obtaining the complex scattering parameters as a function of frequency.

At low frequencies (100 MHz–2 GHz), we used a cell based on the design of Göttmann *et al.*[36] In this cell, the outer coaxial electrode extends several cms from the cable/cell plane, thereby enclosing the liquid sample in the form of a cylindrical column, whereas the inner electrode sticks into the sample as a pin over a distance of 1.8 mm. In the frequency range of 1–30 GHz, a coaxial cut-off disc cell was used where both the coaxial electrodes are terminated at the sample interface. This cell was based on the design of Blackham *et al.*[37,38] A phase-stable coaxial cable (Rhode-Schwartz, ZV-Z96) was connected to the measurement port of the VNA and was calibrated using the accompanying calibration kit (ZV-Z218) employing matched, open, and short standards. Further calibration upon connection of the respective sample cells was performed by measuring the scattering parameters for air and pure water (Milli-Q, 18.2 MΩ cm). For the low-frequency pin-cell, a 4M NaCl solution was further used to shortcut the cell while conductive silver paint (Pelco, Ted Pella, Inc.) was used for short-cutting the cut-off disc cell. A three-term error model[39] was applied to each frequency point, moving the calibration plane from the end of the coaxial cable to the probe/ sample interface. From the corrected parameters the complex permittivities of the liquid samples could be directly calculated.[36,37] All DRS experiments were carried out at 22 °C ± 0.5.

D. Infrared pump-probe spectroscopy

We use vibrational pump-probe spectroscopy to measure the decay of the vibrational anisotropy of the OD-stretch vibration of dilute HDO:H_2O solutions in reverse-micelle samples with $w_0 = 5$ and $c_s = 0.33$ for cyclohexane and $c_s = 0.37$ for *n*-hexane. Isotopically diluted water is prepared by adding 5% D_2O to H_2O. The femtosecond IR pulses used in the experiments [center frequency 2500 cm^{-1}, duration 180 fs (FWHM), energy 5 μJ, spectral width 150 cm^{-1} (FWHM)] are generated by a series of nonlinear frequency-conversion processes that are pumped with the pulses of a commercial Ti:sapphire regenerative amplifier, see Ref. 40 for details. We generate probe and reference beams by splitting off a small portion (~1%) of the IR light with a wedged CaF_2-window. The transmitted light is used as the pump beam.

In the polarization-resolved pump-probe experiments,[40] the pump pulse resonantly excites a small fraction (<10%) of the OD groups to the $v = 1$ state, and the probe pulse is used to measure the resulting absorption change $\Delta\alpha_{||,\perp}(\omega, t)$ as a function of IR-frequency ω and time delay t with respect to the pump pulse. The pump and probe pulses are both linearly polarized, and from the absorption changes observed for parallel ($\Delta\alpha_{\parallel}$) and perpendicular ($\Delta\alpha_{\perp}$) pump and probe polarizations, we construct the isotropic signal

$$\Delta\alpha_{iso}(\omega, t) = \frac{1}{3}(\Delta\alpha_{\parallel}(\omega, t) + 2 \cdot \Delta\alpha_{\perp}(\omega, t)) \qquad (2)$$

and the anisotropy

$$R(\omega, t) = \frac{\Delta\alpha_c(\omega, t)_{\parallel} - \Delta\alpha_c(\omega, t)_{\perp}}{\Delta\alpha_c(\omega, t)_{\parallel} + 2\Delta\alpha_c(\omega, t)_{\perp}}, \qquad (3)$$

where $\Delta\alpha_c(\omega, t)_{\parallel}$ and $\Delta\alpha_c(\omega, t)_{\perp}$ are the parallel and perpendicular transient absorption changes corrected for dynamic heat contributions to the transient spectra. The samples were held between two CaF_2 windows separated by Teflon spacers with a thickness of 250 μm. All experiments were performed at 22 ± 0.5 °C.

III. RESULTS AND DISCUSSION

A. Size and shape of the reverse micelles

1. Spherical reverse micelles

Figure 1 displays small angle x-ray scattering curves for spherical reverse micelles with $w_0 = 2.5, 5$, and 8 at $c_s = 0.33$ and $w_0 = 10$ and 15 at $c_s = 0.28$. A lower c_s for the larger w_0 reverse micelles was chosen to avoid having too high droplet fractions which would result in too viscous reverse micellar solutions. All curves reveal a shape typical for spherical scatterers with a constant intensity at low q and a steep decrease upon approaching the (first) minimum at q_{min}, which allows an estimation of the droplet radius via $r \approx 3\pi/(2q_{min})$. Higher order minima are not visible, since they are smeared out by the polydispersity of the reverse micelles. With increasing w_0 the minimum shifts to smaller scattering vectors q indicating larger droplet sizes, which is also reflected in the increase in the scattering intensity at low q, as the forward scattering scales with the square of the droplet

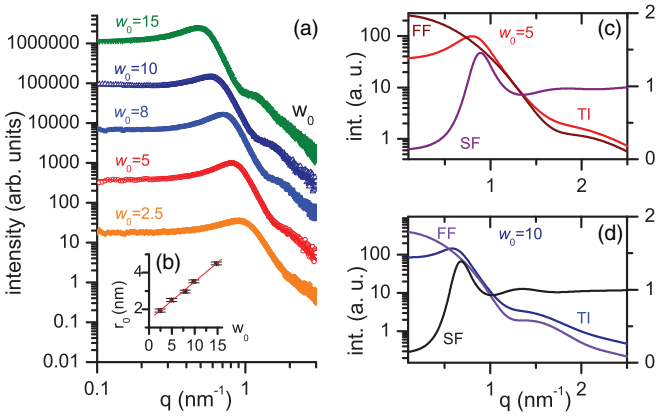

FIG. 1. Small angle x-ray scattering curves (scattering intensity versus the modulus of momentum transfer vector q) from reverse micelles for different w_0 obtained from the water–Igepal–cyclohexane system. (a) Experimental data (symbols) and fits (solid line) for w_0 of 2.5, 5, and 8 at $c_s = 0.333$ and w_0 of 10 and 15 at $c_s = 0.282$ on double logarithmic scale. Successive scattering curves are displaced upwards by one logarithmic unit for better visualization. The shape of the curves is typical for spherical scatterers at concentrations high enough to clearly visualize the structure factor peak. The scattering data were fitted with a multi-component model for hard spheres and the refined parameters are presented in Table I. (b) Linear dependence of the radius r_0 on w_0. The linear regression (red line) yields a proportionality factor ($a = 0.21(1)$ nm) for the water core. (c) and (d) Form factor FF and hard sphere structure factor SF displayed for $w_0 = 5$ and $w_0 = 10$ on semi-logarithmic and linear scale, respectively, that constitute the total scattering of the spherical droplets TI.

volume. Due to the relative high droplet volume fractions a correlation peak shows up at intermediate q, that corresponds to the mean distance of the droplets and thus reveals their interactions (scattering due to droplet interferences).

The scattering curves could be analyzed using a model function based on Vrij's analytical solution for a multicomponent hard sphere system.[30–32] The results from the structural refinement are shown in Table I. Since the electron density of the nonylphenyl surfactant tail is similar to that of cyclohexane, the x-rays see only droplets made up of the ethylene oxide head group moiety and interior water. Plotting the obtained radius r_0 versus w_0 (Figure 1(b)) enables to obtain the proportionality factor a for the linear scaling of the water core radius of the reverse micelles with w_0, with $a = 0.21$nm. The length of the hydrophobic surfactant tail is retrieved from half the droplet surface to surface distance D_0 ($D_0/2 = 0.91(1)$ nm). The values a and D_0 equal those found previously for reverse micelles in the same ternary system at lower c_s.[10] In Figures 1(c) and 1(d), the contributions from the form factor (scattering from a single droplet) and the hard sphere structure factor (droplet interference) are plotted for $w_0 = 5$ and $w_0 = 10$ demonstrating the origin of the observed peaks.

2. Tubular reverse micelles and interconnected networks

For the tubular reverse micelles prepared with $c_s = 0.37$, we measured a scattering curve without significant characteristics. Therefore, we investigated the scattering behavior for $w_0 = 5$ for a series of c_s values. For $c_s < 0.37$, we obtain SAXS curves that show a strong forward scattering

TABLE I. Structure parameters for spherical reverse micelles in the water–Igepal–cyclohexane system obtained from the refinement of the SAXS scattering curves using the multi-component model for hard spheres at different w_0 and RT. The spherical reverse micelles are characterized by the droplet radius r_0, polydispersity parameter σ_0 of the log-normal size distribution, and droplet concentration c_0. For all droplet sizes, a constant surface to surface distance D_0 is found from the hard sphere structure factor, whereby $D_0/2 = 0.91(1)$ nm corresponds to the shell thickness built up by the surfactant tails.

w_0	2.5	5	8	10	15
c_s	0.333	0.333	0.333	0.282	0.282
Vol fraction	0.300	0.3184	0.337	0.300	0.328
c_0 (10^{-3} nm^{-3})	2.641 (1)	1.743 (1)	1.235 (1)	0.725 (1)	0.422 (1)
r_0 (nm)	1.93 (1)	2.50 (1)	2.97 (1)	3.53 (1)	4.50 (1)
σ_0	0.198 (2)	0.166 (2)	0.168 (2)	0.148 (8)	0.160 (8)

compared to the spherical system (see Figure 2). The curves plotted on a double logarithmic scale for $c_s = 0.20$ and 0.14 display at small q a power law dependence of about -1 and $-4/3$, characteristic for stiff rods and semi-flexible worm-like micelles,[33] respectively, whereas the curve for the spherical system at similar volume fraction is flat at low q, as can be seen in Figure 2(b). The two SAXS curves for the cylindrical system could be modeled using the Kholodenko model for worm-like micelles.[33] For $c_s = 0.14$, the fit yields a contour length of 280(66) nm, a Kuhn length L_k of 7.43 (95) nm, and a radius for the cylindrical cross-section r_c of 2.55 (1) nm with a log-normal size distribution $\sigma_0 = 0.096$ (9). The Kuhn length indicates the length over which the chain of the worm-like reverse micelles is not curved. The minimum observed corresponds in this case to the radius of the cross-section that displays a lower polydispersity than observed for the spheres. For $c_s = 0.20$, the contour length has decreased to 105(26) nm, which can be seen from the lowering in the forward scattering at small q, whereas the Kuhn length ($L_k = 6.83(99)$ nm) and the cross-sectional radius ($r_c = 2.55(2)$ with $\sigma_0 = 0.115(3)$) do not change significantly. At high q the curves for the spherical and the cylindrical reverse micelles fall on top of each other at comparable volume fractions. The red curve in Figure 2(b) for $c_s = 0.14$ stems from spherical micelles with $r_0 = 2.88(4)$ nm and $\sigma_0 = 0.177(2)$ showing mainly droplet form factor scattering.

Upon increasing the concentration for the tubular system, the intensity decreases at low q, showing a slope <-1 already for $c_s = 0.27$ (not shown) at low q. At intermediate q, a peak starts to develop at $c_s = 0.37$, whereby a shoulder can already be observed at $c_s = 0.32$ on linear scale (Figure 2(a)). For the highest c_s values of 0.46 and 0.56 that correspond to volume fractions of 0.40 and 0.50, respectively, the peak that is characteristic for bicontinuous structures or sponge phases is fully developed. All the curves for the cylindrical system show a minimum at high q that hardly changes its value. This indicates that the radius of the cross-section stays nearly constant. With increasing surfactant concentration the cylindrical reverse micelles interlink and form branch points, whereby passages between the individual water channels are created leading finally to a network of interconnected water channels that span the whole volume forming meshes within the oil.[41] For these structures, we cannot anymore resort to liquid state theories to analyze the scattering as in the case of the spheres and isolated closed cylinders. In this case, random surface models come into play that are based on Landau theory.[42,43] Here, we use the phenomenological model proposed by Teubner and Strey in which Gaussian fluctuations of the order parameter field determine the scattering intensity in the vicinity of the peak[34] to estimate the domain size and the correlation length of the structures formed at $c_s \geq 0.46$. The fits reveal a domain size d of 7.1 nm and 6.4 nm for $c_s = 0.46$ and 0.56, respectively, and a correlation length $\leq$4.5 nm for both systems.

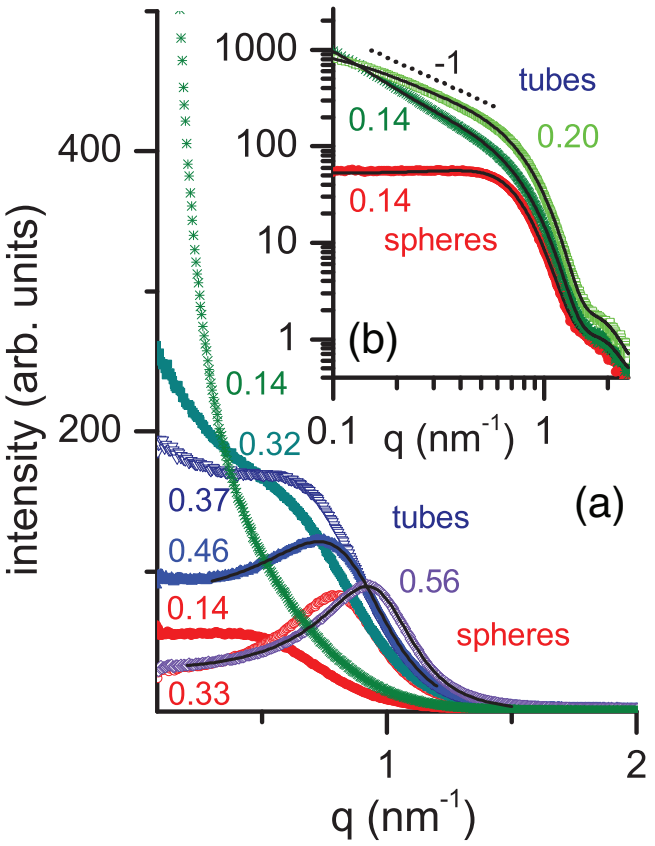

FIG. 2. Small angle x-ray scattering curves from reverse micellar aggregates for both ternary systems, i.e., water–Igepal–cyclohexane (spheres) and water–Igepal–hexane (tubes), as a function of c_s at a constant w_0 of 5. The green and blue scattering curves for $c_s = 0.14$, 0.2, 0.32, 0.37, 0.46, and 0.56 belong to the tube system, whereas the red scattering curves for the sphere system at $c_s = 0.14$ and 0.33 are added for comparison. (a) Development of the peak typical for bicontinuous microemulsions or sponge phases from long semi-flexible worm-like reverse micelles on linear scale. (b) Scattering curves for long cylindrical micelles for $c_s = 0.14$ and 0.2 for the water–Igepal–hexane system on double logarithmic scale. The inserted dashed line with a slope of -1 indicates the q^{-1} power law decay characteristic for stiff rods. The black solid lines display fits obtained applying the Kholodenko model for long semi-flexible worm-like scatterers at $c_s = 0.14$ (olive stars) and $c_s = 0.20$ (light green open squares) in (b) and fits to the peak region obtained by the Teubner-Strey model for $c_s = 0.46$ (upright blue filled triangles) and $c_s = 0.56$ (violet open diamonds) in (a).

We thus find that depending on the apolar phase (*n*-hexane or cyclohexane) our samples contain either spherical or cylindrical reverse micelles. For the spherical micelles, the radius is proportional to w_0. Earlier studies have shown that the radius of infinitely long cylindrical reverse micelles

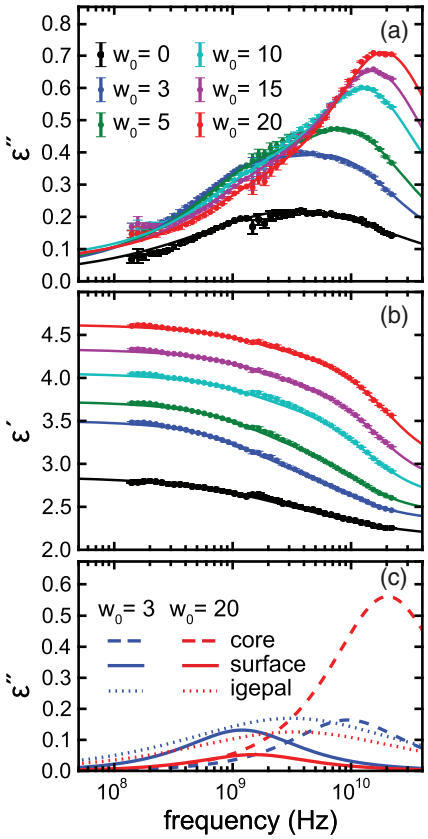

FIG. 3. Imaginary (a) and real (b) parts of the dielectric permittivity of spherical reverse micelles of different sizes (w_0 = 3–20) for the water–Igepal–cyclohexane system. The solid lines represent least-squares fits to the data using Eq. (4). (c) Igepal (dotted), surface-water (solid), and core-water (dashed) contributions to the dielectric permittivity for $w_0 = 3$ (blue) and $w_0 = 20$ (red).

converges to 2/3 the radius of spherical reverse micelles of the same w_0.[27,28,44]

B. Dynamics of water in nanoscopic spheres

In Figure 3, we show the real and imaginary parts (ϵ' and ϵ'', respectively) of the relative permittivity for a series of solutions containing spherical reverse micelles with increasing w_0 values. For $w_0 = 0$ (surfactant only), we observe a broad band in the $\epsilon''(\omega)$ spectrum, which we attribute to the dipolar reorientation of the surfactant (Igepal) molecules. For nonzero w_0, we observe an additional feature at higher frequencies, which we assign to reorientation of the water in the reverse micelles. This additional component grows in intensity and shifts to higher frequency with increasing w_0 (increasing water content), approaching ~20 GHz for the largest micelles, i.e., close to the value of the main relaxation mode of bulk liquid water.[45]

We find that the water dielectric response can be well described as a sum of contributions from water at the surface of the micelle and water in the core of the micelle, with the two types of water exhibiting distinctly different reorientation dynamics: the interfacial water molecules that hydrate the hydrophilic moiety of the surfactant show significantly slower dynamics than bulk liquid water, whereas water in the core of the nanoscopic volume behaves similar to bulk water. Such a core/shell model is certainly a simplification, and molecular dynamics simulations indeed show a gradual transition in reorientation time constant going from the surface to the core.[46,47] Nevertheless, our experimental results show that the distribution of reorientation times is approximately bimodal, as has been observed before for a wide range of reverse micellar systems, with both ionic and nonionic surfactants.[3–11,48–50]

The total frequency-dependent complex permittivity $\epsilon(\omega)$ of the reverse micellar system is thus modeled as a sum of the contributions of Igepal, core water, surface water, and cyclohexane

$$\epsilon(\omega) = \epsilon_{\text{core}}(\omega) + \epsilon_{\text{surface}}(\omega) + \epsilon_{\text{Igepal}}(\omega) + \epsilon_{\infty}, \tag{4}$$

where $\epsilon_i(\omega)$ are the complex permittivities of the individual components, and ϵ_∞ is the permittivity in the high-frequency limit. ϵ_∞ includes the cyclohexane response, which is purely real and independent of frequency in the range of frequencies investigated here. We model the surface and core water responses as Debye relaxation modes,

$$\epsilon_i(\omega) = \frac{\Delta\epsilon_i}{1 + i\omega 2\pi\tau_{\text{D},i}} \tag{5}$$

with $i \in \{\text{core}, \text{surface}\}$. The Igepal contribution has a broader spectrum, and can be well described by a Cole-Cole mode,[51]

$$\epsilon_{\text{Igepal}}(\omega) = \frac{\Delta\epsilon_{\text{Igepal}}}{(1 + i\omega 2\pi\tau_{\text{D,Igepal}})^{(1-\alpha)}}. \tag{6}$$

In these equations, $\Delta\epsilon_i$ are the permittivity amplitudes, and $\tau_{\text{D},i}$ Debye relaxation time constants of the individual components. From a least-squares fit of a Cole-Cole mode to the $w_0 = 0$ data, we obtain $\tau_{\text{D,Igepal}} = 50(1)$ and 47(1) ps, and $\alpha = 0.35(1)$ and 0.35(1) for $w_s = 0.33$ and 0.29, respectively (where the numbers in parentheses indicate the 1σ uncertainties in the last digit). These values were kept constant in the least-squares fits to the data for $w_0 > 0$. We performed a simultaneous least-squares fit of Eq. (4) to the real and the imaginary components of the dielectric relaxation spectra for all w_0, treating $\tau_{\text{D,Igepal}}$ as a fixed parameter, and assuming a linear relation between $\Delta\epsilon_{\text{D,Igepal}}$ and the volume fraction of Igepal. The results of the fit are shown by the solid lines in Figure 3, where panel (a) and (b) show the imaginary and real parts of the permittivity respectively, and panel (c) the decomposition of the imaginary part into the contributing modes for the smallest and largest micelles studied ($w_0 = 3$ and 20). The fit parameters are presented in Figure 4.

The surface-water Debye time constants vary between 132(5) ps for $w_0 = 3$ and 105(9) ps for $w_0 = 20$ thus showing only a weak dependence on micelle size, see Figure 4(a) (indicated by the dashed blue line).[65] These surface-water reorientation times are more than one order of magnitude slower than the Debye time of bulk water (8.38 ps at 298 K).[45] The water molecules giving rise to the surface-water Debye mode are likely hydrogen bonded to the outer oxygen atoms of the surfactant head groups. This assignment is consistent with the observation that the surface-water reorientation time is only weakly dependent on the micelle size. The core water

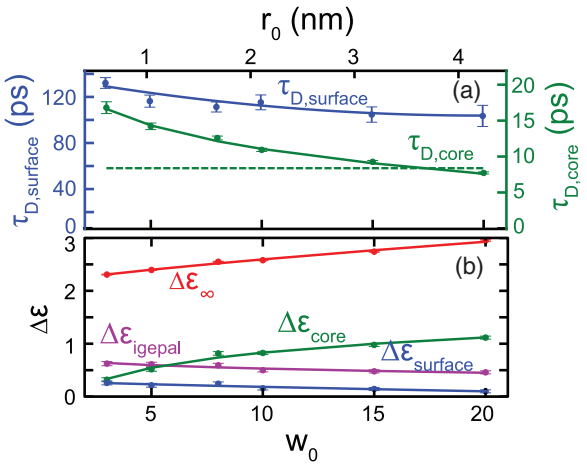

FIG. 4. Fit parameters obtained from a global least-squares fit of Eq. (4) to the data shown in Fig. 3. (a) Surface-water and core-water Debye relaxation times as a function of w_0. (b) Amplitudes $\Delta\epsilon_{\mathrm{D,Igepal}}$, $\Delta\epsilon_{\mathrm{D,H_2O}}$, and ϵ_∞ as a function of w_0. The small discontinuity between $w_0 = 8$ and $w_0 = 10$ is due to a change in c_s from 0.33 (for $w_0 \leq 8$) to 0.29 (for $w_0 \geq 10$). The curves are a guide to the eye.

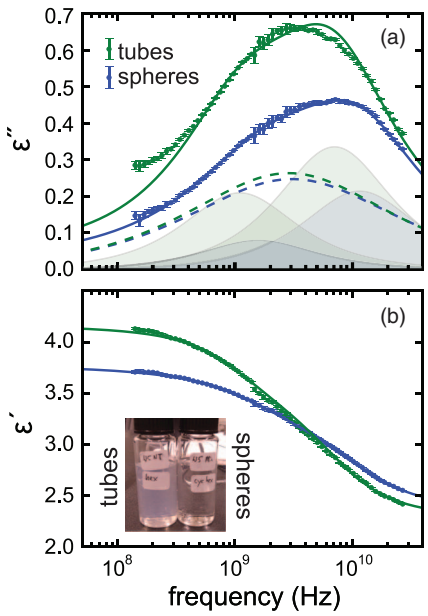

FIG. 5. The imaginary (a) and the real (b) parts of the dielectric response of tubular reverse micelles (green, water–Igepal–hexane) compared to spherically shaped reverse micelles (blue, water–Igepal–cyclohexane). The solid lines represent least-squares fits to the data using Eq. (4). The fits are composed of the Igepal contribution (dashed lines), the surface-water contribution (filled curves at low frequency), and the core water contribution (filled curves at high frequency). (Inset) Photo showing a sample of tubular (left) and spherical (right) reverse micellar system.

reorientation time decreases monotonically with increasing size, from 16.0(4) ps for $w_0 = 3$ to 8.2(1) ps for $w_0 = 20$.

In previous IR pump-probe studies, it was found that the reorientation dynamics of the OD groups of dilute HDO:H_2O in reverse micelles can be well described assuming a core-water reorientation time equal to that of bulk water for all micelle sizes.[9,10,52] However, attempts to fit the dielectric-relaxation data in the same manner (keeping $\tau_{\mathrm{D,\,core}}$ fixed to the bulk reorientation time of water) were not successful. The difference in w_0 dependence of the orientational correlation times of the core water obtained from dielectric relaxation and IR pump-probe spectroscopy suggests that the reorientation dynamics of the permanent dipole moment of water molecules (giving rise to the dielectric relaxation) might be more sensitive to nanoconfinement than the reorientation dynamics of OD bonds of isolated HDO molecules (as observed in the IR pump-probe measurements). This difference might be due to the different consequences of the truncation of the hydrogen-bond network at the surface of the nanoscopic volume for the two types of reorientation. The observed difference might then be similar to the different changes in the permanent-dipole-moment and OD-bond reorientation dynamics observed upon adding salts to bulk water.[53] Finally, in Figure 4(b) we observe that ϵ_∞ and the core water response $\Delta\epsilon_{\mathrm{core}}$ both increase (and in a similar manner) with increasing water content w_0. On the other hand, $\Delta\epsilon_{\mathrm{Igepal}}$ and $\Delta\epsilon_{\mathrm{surface}}$ decrease slightly as the Igepal concentration decreases slightly upon adding water.

C. Comparison between nanoscopic spheres and cylinders

By using *n*-hexane instead of cyclohexane as polar solvent, we prepare cylindrical instead of spherical micelles with the same value of w_0 (see Sec. II B). The difference in nanoscopic morphology of the samples causes a directly visible difference in the samples, see inset of Fig. 5(b): the sample containing cylindrical reverse micelles shows faint blue light scattering which is not observed in the sample with spherical reverse micelles. The cylinders are sufficiently long to cause significant Rayleigh scattering. In Figure 5, we also compare the dielectric response of spherical and cylindrical reverse micelles, both with $w_0 = 5$. Surprisingly, the response of water in nano-cylinders is much larger than that of water in nano-spheres. We find that the dielectric response of both the cylindrical and spherical micelles can be modeled by Eq. (4). The fits are shown in Figure 5, where we also indicate the individual contributions of the surface water and the core water for the tubes (green fill) and spheres (blue fill); the parameters obtained from the fit are given in Table II. We find that the reorientation of the core water in cylindrical micelles is slowed down compared to that in spherical micelles ($\tau_{\mathrm{D,\,core}} = 21.8$ vs. 13.7 ps), and that the corresponding amplitude of the dielectric response is increased ($\Delta\epsilon_{\mathrm{core}} = 0.65$ vs. 0.43). The most prominent difference between cylindrical and spherical micelles is the much

TABLE II. Fit results for the dielectric response of reverse micelles in tubular and spherical geometry for $w_0 = 5$ for the systems water–Igepal–hexane (tubes, green) and water–Igepal–cyclohexane (spheres, blue). $\tau_{D,c}$ and $\tau_{D,s}$ are the core and surface water reorientation times and $\Delta\epsilon_c$ and $\Delta\epsilon_s$ are the dielectric response of core and surface water for spherical and tubular micelles. The uncertainties are 1σ.

	$\tau_{D,\,c}$ (ps)	$\tau_{D,\,s}$ (ps)	$\Delta\epsilon_c$	$\Delta\epsilon_s$
Spheres	13.7(2)	101(1)	0.43(3)	0.16(3)
Tubes	21.8(4)	140(2)	0.65(1)	0.43(1)

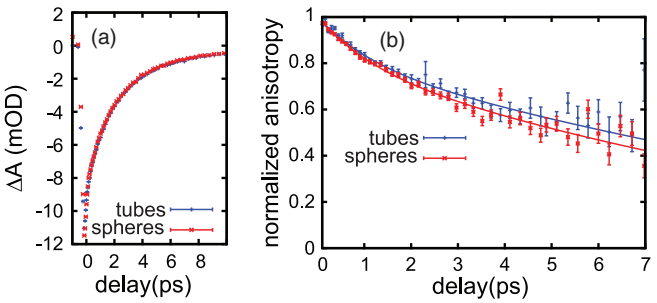

FIG. 6. (a) Isotropic decay of the pumped OD stretch vibration at 2525 cm^{-1} of tubes and spheres. (b) The anisotropy decay of the OD-stretch mode of dilute HDO:H_2O in tubular and spherical reverse micelles. To improve the signal-to-noise ratio, the data were averaged over a probe-frequency range from 2525 to 2570 cm^{-1} over which no discernible frequency dependence was observed.

larger amplitude of the surface-water dielectric response of the cylinders: $\Delta\epsilon_{D,\,surface} = 0.43$ vs. 0.16. The slower Debye relaxation time for core water in cylinders as compared to that in spheres can be understood on the basis of our observation that the reorientation dynamics of the core water in reverse micelles slows down with decreasing micelle size (see Figure 4(a)). Since for cylinders and spheres with the same w_0 (=surface/volume ratio) the radius of the cylinders is approximately 2/3 of the radius of the spheres, one may therefore expect slower reorientation dynamics in the cylindrical than in the spherical reverse micelles, as is indeed observed.

The difference in amplitude of the dielectric response of the tubes and the spheres cannot be due to a difference in chemical composition of the samples, as the compositions are exactly identical apart from the apolar solvents, cyclohexane and *n*-hexane, which do not show a frequency-dependent dielectric response in the investigated frequency region. To investigate if the difference in dielectric response might be due to a difference in the fractions of surface and core water in the two types of reverse micelle, we prepared reverse micelles containing dilute (10%) HDO:H_2O mixtures, and investigated the orientational relaxation of the OD groups using polarization-resolved vibrational pump-probe spectroscopy, which provides a direct determination of the fractions of surface and core water. This is because the surface-water molecules reorient much more slowly than the core-water molecules,[3–11] so that the OD-stretch vibrational anisotropy decays in a bimodal manner, with the amplitudes of the fast and the slow relaxation being proportional to the fractions of the core and surface water, respectively. In Figure 6(a), we show the isotropic transient-absorption changes of HDO molecules in cylindrical and spherical reverse micelles as a function of delay, measured at the maximum of the OD-stretch band at 2525 cm^{-1}. The overlapping delay traces show that there is no significant difference in the vibrational relaxation dynamics between the cylindrical and spherical reverse micelles. In Figure 6(b), we plot the normalized anisotropy decay of the two systems. The anisotropy decays are bimodal and show quite similar fast and slow components for the two systems. From a global least-squares fit to the anisotropy decay and isotropic signals (see Ref. 10 for details of the fit procedure), we obtain the fit parameters listed in Table III. The

TABLE III. Fit results for the anisotropic and isotropic decay of the OD-stretch vibration in tubular and spherical reverse micelles. S is the core water fraction, $T_{1,i}$ is the vibrational relaxation time of Igepal and surface water, $\tau_{IR,\,s}$ is the surface-water reorientation time, and R_0 is the initial (zero-delay) value of the anisotropy. Note that since the slow reorientation times exceed our accessible time window, only lower limits for their values can be given. The values in parentheses indicate the uncertainties (1σ) in the last digit.

	$T_{1,\,Igepal}$ (ps)	$T_{1,\,s}$ (ps)	$\tau_{IR,\,s}$ (ps)	S	R_0
Spheres	0.73(6)	4.2(1)	>9(1)	0.30(3)	0.33(1)
Tubes	1.1(2)	4.3(3)	>10(1)	0.30(3)	0.34(1)

fits are shown as solid curves in Fig. 6. We find that the amplitude ratios of the slow and fast components in the anisotropy dynamics are identical for cylindrical and spherical reverse micelles within the experimental uncertainties (2σ). It thus follows that the fractions of surface and core water are the same in the two types of micelles, and that their OD-stretch reorientation dynamics are the same. This notion is corroborated by the similar vibrational relaxation dynamics of the two samples since core and surface-water molecules have different vibrational lifetimes,[10] so that a difference in core/surface ratio should have caused a difference in the observed relaxation dynamics. Finally, the near-identical FTIR spectra of the two samples (shown in Figure 7) also indicate a very similar core/surface ratio in the two systems, as is to be expected from geometrical considerations.[66] Surface-bound water molecules generally have a higher OD-stretch frequency than core water molecules, so that a difference in surface/core ratio would have been observable as a difference in the shape and maximum of the OD-stretch absorption band.[4,10] We therefore conclude that the observed strong difference in dielectric response of cylindrical and spherical reverse micelles cannot be caused by a difference in the fractions of surface and core water.

D. Effect of the shape of nanoscopic water volumes on the dielectric response

A hint as to the origin of the very different dielectric responses of water in nanoscopic cylindrical and spherical

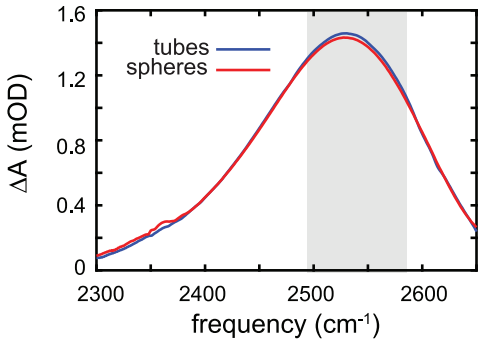

FIG. 7. Absorption difference spectrum OD stretch in 10% HDO in H_2O in reverse micelles with $w_0 = 5$ in cyclohexane (spheres) and *n*-hexane (tubes). The intensity of the OD stretch in spheres is 2% lower than in the tubes. This difference lies within the error of the preparation.

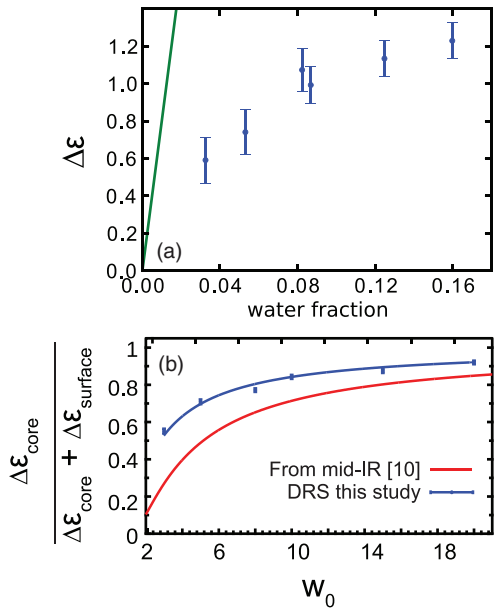

FIG. 8. (a) The water contribution to the dielectric response $\Delta\epsilon_{water}$ vs. the water fraction. The green solid line is the response predicted assuming a linear dependence of $\epsilon_{0,bulk,H_2O}$ with the water volume fraction. (b) Relative amplitude of the core-water dielectric response with respect to the total water response (blue points), compared to the core-water fraction as obtained from previous IR pump-probe data (red curve).[10]

reverse micelles is provided by the absolute magnitude of these responses. The amplitude of the dielectric response of the spherically nanoconfined water is much smaller than would be expected from its volume fraction. This can be seen directly from the total water contribution $\Delta\epsilon_{water} = \Delta\epsilon_{surface} + \Delta\epsilon_{core}$ obtained from the fits. In Figure 8(a) we show $\Delta\epsilon_{water}$ as a function of the water fraction for the different reverse micelle sizes.

The dielectric response of the nanoconfined water is clearly much less than would be expected based on the water volume fraction (these expected values are shown as the green line). For example, the sample containing reverse micelles of $w_0 = 8$ contains 8% vol. water, and would be expected to have a water contribution to the dielectric constant of about 6, whereas we observe an $\Delta\epsilon_{water}$ of only 1. Previous studies have demonstrated a similar reduction of the dielectric response in reverse micellar systems.[54,55]

It is well known that the dielectric constants of mixtures, e.g., emulsions, can differ significantly from a weighted sum of the responses of the pure constituents as a result of local field effects.[56] These local-field effects can be accounted for by describing the mixture with a so-called effective medium approach in which it is assumed that the constituents are homogeneously distributed over the mixture. For emulsions of water, well-known effective medium approaches like the Maxwell-Garnett and Bruggeman models are not applicable as these models are based on a description of local-field effects with the Lorentz local field. The Lorentz local field description is only valid for systems for which the dielectric response is governed by the polarizability of the atoms/molecules. However, the dielectric response of water is dominated by the reorientation of molecular dipoles, for which the Onsager local field $E_{local} = [3\epsilon/(2\epsilon + 1)]E$ applies. The Onsager local field of water undergoes only a small change when water is dispersed in an apolar solvent.[67] Hence, local-field effects cannot account for the large attenuation of the dielectric response, which occurs when water is confined in nanoscopic volumes.

The dielectric response of dipolar systems depends strongly on the local ordering of the contributing dipoles and their correlated motion. This effect of local ordering is usually accounted for by the so-called Kirkwood correlation factor g_K, which is linearly proportional to ϵ,[57,58]

$$\epsilon \propto g_K \mu^2,$$

where μ is the dipole moment of a single molecule. In the absence of local orientational order $g_K = 1$, whereas $g_K > 1$ if the dipole moments of neighboring molecules tend to align. In the case of antiparallel neighboring dipole moments $g_K < 1$. In bulk liquid water and ice, the Kirkwood factor is quite large and attains a value of ~3 as a result of the (near-)tetrahedral arrangement of the water dipoles.[57,59,60] In nanoconfined water however, the Kirkwood factor can be much smaller. Simulations by Senapati and Chandra have shown a 50% reduction of ϵ_{H_2O} for very small (0.61 nm radius) spherical water volumes that have no electrostatic interaction with the confining walls.[61] We believe that this reduction of the Kirkwood factor is due to an anti-parallel orientation of water molecules at opposing surfaces of the nanodroplet. In reverse micelles, the OH bond and dipoles of the water molecules at the surface point radially outward in order to hydrate the oxygen atoms of the Igepal surfactant. Because of the spherical symmetry of water volume, this configuration corresponds to a largely anti-parallel arrangement of the water dipole moments, resulting in a very small Kirkwood factor g_K (this might be compared to a hydration shell around a cation, which also has a very small Kirkwood factor because of the canceling dipole moments[62,63]). The water molecules at the inside of the reverse micelles need to accommodate their hydrogen-bond structure to the structure of the surface water and to each other, which results in a hydrogen-bond network that is significantly distorted from an ideal tetrahedral structure. Hence, the Kirkwood g_K factor of the core water is also expected to be much smaller than of bulk liquid water. The observed dielectric constant of the reverse micelles is about 6 times smaller (see above) than the value predicted based on the bulk-water dielectric constant, meaning that our results suggest that the Kirkwood correlation factor of nanoconfined water is about 6 smaller than that of bulk water, i.e., smaller than unity. The fact that the water nanospheres with hydrophobic surfaces studied by Senapati and Chandra[61] also show a strong reduction in g_K suggests that the main conditions for reducing the Kirkwood factor are the small size and centrosymmetric shape of the water nanodroplet. Interestingly, the simulations of Senapati and Chandra show that for hydrophobic surfaces the reduction in g_K already disappears at comparatively small droplet sizes ($\epsilon = 71$ for $r_0 = 1.2$ nm),[61] whereas we find a reduction in g_K that persists up to larger droplet sizes (see Fig. 4(b)). If our hypothesis is correct, then this difference suggests that the disruption of the hydrogen-bond structure of water extends deeper for a hydrophilic surfactant surface than

for a hydrophobic surface, for which it seems to be a more local effect.

With increasing size of the reverse micelles, the relative contribution of the core component increases with respect to that of the surface component, as can be seen in Fig. 8(b), where we plot the relative contribution of the core water with respect to the total water response, $\frac{\Delta\epsilon_{\text{core}}}{\Delta\epsilon_{\text{core}}+\Delta\epsilon_{\text{surface}}}$, as a function of w_0. This relative increase of the core component with increasing micelle size is in itself not surprising, and is in line with the core/shell model.

However, when we compare the relative dielectric-response contribution of the core water to its molar fraction, [core]/([core]+[surface]) (obtained from previous time-resolved IR measurements[10]), we find that the dielectric response of the core water is always larger than its molar fraction (with increasing w_0 both fractions eventually approach unity, and the difference vanishes). This discrepancy suggests that just as the Kirkwood correlation factor of bulk water is larger than that of micellar core water (see previous paragraph), the Kirkwood factor of the core water is larger than that of the surface water. The very low Kirkwood factor of the surface-water molecules can be well explained from the approximately antiparallel arrangement of water molecules at the opposing surfaces of the nanodroplet, as discussed above.

The change in the Kirkwood factor upon nanoconfinement can also account for the difference in the amplitudes of the dielectric responses of water in spherical and cylindrical reverse micelles. In a sphere, every dipole moment of a water molecule at the surface can in principle be canceled by that of a water molecule on the opposite side, but in a cylinder the components of the water dipole moments along the cylinder axis may (at least locally) add up, which would cause the Kirkwood factor to be larger for the surface water of a cylinder than for that of a sphere. In addition, the hydrogen-bond network of water at the surface of a cylinder is probably less distorted from the ideal tetrahedral structure than at the surface of a sphere, because the former has curvature in only one surface dimension, and the latter in both, again causing the Kirkwood factor of surface water to be larger in the former than in the latter. Both effects will lead to a much larger amplitude of the dielectric response of surface water in cylindrical reverse micelles as compared to spherical reverse micelles. The effects of alignment of the surface water will propagate into the core water, but the effects will be less pronounced, which implies that the core water of the cylindrical micelles will have a larger dielectric response than the core water of the spherical micelles, but the difference is smaller than for the surface water.

The effects of nanoconfinement on the water structure and thus on the dielectric response are strongly dependent on the nature of the interactions between the water molecules and the embedding structure. In case this structure is formed by a layer of surfactant molecules, the interactions are hydrophilic, and in the case of a closed structure the water molecules at opposite sides in the surface layer will arrange in an anti-parallel configuration. In case the embedding structure is hydrophobic and not spherical, the parallel arrangement of the water dipoles can be enhanced in comparison to bulk water. Indeed, experiments on water in carbon nanotubes revealed an even higher Kirkwood factor than for bulk liquid water, and thus a relatively large dielectric response.[64]

IV. CONCLUSIONS

We studied the dielectric relaxation of liquid water in nanoscopic volumes of different sizes and shapes. Nanoscopic water volumes were formed within reverse micelles in an apolar matrix using Igepal as surfactant. The dielectric response of the nanoconfined water under these conditions can be well described as a sum of the responses of a surface-bound water fraction and a core water fraction. The Debye relaxation time constant of the surface water is found between 132(6) ps for $w_0 = 3$ and 105(9) ps $w_0 = 20$ and shows only a weak dependence on the size of the nanoscopic volume. The time constant of the core water, on the other hand, decreases from 16.0 ± 0.4 ps for reverse micelles for $w_0 = 3$ to 8.2 ± 0.1 ps for $w_0 = 20$. Although the simple core/shell model provides a good quantitative description of our data, we should point out that a detailed description would require more detailed modeling along the lines of Ref. 46, and we hope that our results will stimulate work in this direction.

We demonstrated that the shape of the reverse micelles can be modified by varying the apolar solvent. Using small-angle x-ray scattering, we found that the reverse micelles acquire a cylindrical shape if *n*-hexane is used as solvent. The Debye relaxation is slower in cylindrical than in spherical nanoscopic volumes having the same surface/volume fraction. Furthermore, the amplitude of the dielectric response is larger in cylindrical than in spherical volumes, in particular for the water located at the surface. We thus find that the shape of a nanoscopic volume of water strongly affects its dielectric response.

The difference in dielectric response between cylindrical and spherical nanoscopic volumes is not due to a difference in the fractions of surface and core water (as is demonstrated by the vibrational pump-probe measurements), or to local-field effects. Rather, we explain this difference from the interaction of the surface-water molecules with the surfactant molecules, which tends to align the surface-water dipoles in such a way that they are anti-parallel for opposing spherical surfaces, but less for opposing cylindrical surfaces. Similar alignment effects will occur in any kind of nanoconfined water (the details depending on the molecular properties and shape of the confining material), and may be expected to have a significant influence on the spatial distribution and transport properties of ions in nanoscopic channels and vesicles.

ACKNOWLEDGMENTS

This work is part of the research program of the Stichting voor Fundamenteel Onderzoek der Materie (FOM), financially supported by the Nederlandse organisatie voor Wetenschappelijk Onderzoek (NWO). The authors would like to thank H. Schoenmaker and H. J. Boluijt for technical support as well as Johannes Hunger and Jiri Oen for valuable discussions. N.O. gratefully acknowledges the European Commission (FP7) for funding through the award of a Marie Curie fellowship.

[1] N. Nandi and B. Bagchi, J. Phys. Chem. B **101**, 10954 (1997).
[2] R. McIntosh, D. Nicastro, and D. Mastronarde, Trends Cell Biol. **15**, 43 (2005).
[3] R. E. Riter, D. M. Willard, and N. E. Levinger, J. Phys. Chem. B **102**, 2705 (1998).
[4] A. M. Dokter, S. Woutersen, and H. J. Bakker, Phys. Rev. Lett. **94**, 178301 (2005).
[5] S. Schrödle, G. Hefter, W. Kunz, and R. Buchner, Langmuir **22**, 924 (2006).
[6] I. R. Piletic, D. E. Moilanen, D. B. Spry, N. E. Levinger, and M. D. Fayer, J. Phys. Chem. A **110**, 4985 (2006).
[7] M. A. Sedgwick, D. C. Crans, and N. E. Levinger, Langmuir **25**, 5496 (2009).
[8] A. M. Dokter, S. Woutersen, and H. J. Bakker, Proc. Natl. Acad. Sci. U.S.A. **103**, 15355 (2006).
[9] E. E. Fenn, D. B. Wong, and M. D. Fayer, Proc. Natl. Acad. Sci. U.S.A. **106**, 15243 (2009).
[10] T. H. van der Loop, M. R. Panman, S. Lotze, J. Zhang, T. Vad, H. J. Bakker, W. F. C. Sager, and S. Woutersen, J. Chem. Phys. **137**, 044503 (2012).
[11] A. Patra, T. Q. Luong, R. K. Mitra, and M. Havenith, Phys. Chem. Chem. Phys. **16**, 12875 (2014).
[12] J. Teixeira, J.-M. Zanotti, M.-C. Bellissent-Funel, and S.-H. Chen, Physica B **234–236**, 370 (1997).
[13] I. M. Briman, D. Rébiscoul, O. Diat, J.-M. Zanotti, P. Jollivet, P. Barboux, and S. Gin, J. Phys. Chem. C **116**, 7021 (2012).
[14] A. Taschin, P. Bartolini, A. Marcelli, R. Righini, and R. Torre, Faraday Discuss. **167**, 293 (2013).
[15] M. Sattig, S. Reutter, F. Fujara, M. Werner, G. Buntkowsky, and M. Vogel, Phys. Chem. Chem. Phys. **16**, 19229 (2014).
[16] G. Hummer, J. C. Rasaiah, and J. P. Noworyta, Nature (London) **414**, 188 (2001).
[17] G. Hummer, Mol. Phys. **105**, 201 (2007).
[18] J. C. Rasaiah, S. Garde, and G. Hummer, Annu. Rev. Phys. Chem. **59**, 713 (2008).
[19] K. Schmidt-Rohr and Q. Chen, Nat. Mater. **7**, 75 (2008).
[20] V. Crupi, D. Majolino, P. Migliardo, V. Venuti, and M. C. Bellissent-Funel, Mol. Phys. **101**, 3323 (2003).
[21] M. Erko, G. H. Findenegg, N. Cade, A. G. Michette, and O. Paris, Phys. Rev. B **84**, 104205 (2011).
[22] S. M. Chathoth, E. Mamontov, A. I. Kolesnikov, Y. Gogotsi, and D. J. Wesolowski, Europhys. Lett. **95**, 56001 (2011).
[23] A. A. Milischuk and B. M. Ladanyi, J. Chem. Phys. **135**, 174709 (2011).
[24] S. Safran, L. Turkevich, and P. Pincus, J. Phys. Lett. **45**, 69 (1984).
[25] L. K. Shrestha, T. Sato, D. P. Acharya, T. Iwanaga, K. Aramaki, and H. Kunieda, J. Phys. Chem. B **110**, 12266 (2006).
[26] S. May and A. Ben-Shaul, J. Phys. Chem. B **105**, 630 (2001).
[27] E. M. Blokhuis and W. F. C. Sager, J. Chem. Phys. **115**, 1073 (2001).
[28] W. F. C. Sager, *Nanostructured Soft Matter*, edited by A. V. Zvelindovsky (Springer, Netherlands, 2007), pp. 3–44.
[29] A. Patra, T. Q. Luong, R. K. Mitra, and M. Havenith, Phys. Chem. Chem. Phys. **15**, 930 (2013).
[30] A. Vrij, J. Chem. Phys. **71**, 3267 (1979).
[31] D. Gazzillo and A. Giacometti, J. Chem. Phys. **113**, 9837 (2000).
[32] T. Vad, H.-G. Haubold, N. Waldöfner, and H. Bönnemann, J. Appl. Crystallogr. **35**, 459 (2002).
[33] A. L. Kholodenko, Macromolecules **26**, 4179 (1993).
[34] M. Teubner and R. Strey, J. Chem. Phys. **87**, 3195 (1987).
[35] J. S. Pedersen, Adv. Colloid Interface Sci. **70**, 171 (1997).
[36] O. Göttmann, U. Kaatze, and P. Petong, Meas. Sci. Technol. **7**, 525 (1996).
[37] D. Blackham and R. D. Pollard, IEEE Trans. Instrum. Meas. **46**, 1093 (1997).
[38] W. Ensing, J. Hunger, N. Ottosson, and H. J. Bakker, J. Phys. Chem. C **117**, 12930 (2013).
[39] M. Hiebel, *Fundamentals of Vector Network Analysis* (Rohde & Schwarz USA, Inc., 2005).
[40] S. van der Post and H. J. Bakker, Phys. Chem. Chem. Phys. **14**, 6280 (2012).
[41] T. Foster, S. A. Safran, T. Sottmann, and R. Strey, J. Chem. Phys. **127**, 204711 (2007).
[42] L. Arleth, S. Marcelja, and T. Zemb, J. Chem. Phys. **115**, 3923 (2001).
[43] M. Peltomäki, G. Gompper, and D. Kroll, J. Chem. Phys. **136**, 134708 (2012).
[44] D. I. Svergun, P. V. Konarev, V. V. Volkov, M. H. J. Koch, W. F. C. Sager, J. Smeets, and E. M. Blokhuis, J. Chem. Phys. **113**, 1651 (2000).
[45] R. Buchner, J. Barthel, and J. Stauber, Chem. Phys. Lett. **306**, 57 (1999).
[46] P. A. Pieniazek, Y.-S. Lin, J. Chowdhary, B. M. Ladanyi, and J. L. Skinner, J. Phys. Chem. B **113**, 15017 (2009).
[47] A. A. Bakulin, D. Cringus, P. A. Pieniazek, J. L. Skinner, T. L. C. Jansen, and M. S. Pshenichnikov, J. Phys. Chem. B **117**, 15545 (2013).
[48] A. Das, A. Patra, and R. K. Mitra, J. Phys. Chem. B **117**, 3593 (2013).
[49] T. Sato, H. Sakai, K. Sou, R. Buchner, and E. Tsuchida, J. Phys. Chem. B **111**, 1393 (2007).
[50] R. Biswas, N. Rohman, T. Pradhan, and R. Buchner, J. Phys. Chem. B **112**, 9379 (2008).
[51] R. Kubo, M. Toda, and N. Hashitsume, *Statistical Physics II. Nonequilibrium Statistical Mechanics* (Springer, Berlin, 1985).
[52] A. M. Dokter, S. Woutersen, and H. J. Bakker, J. Chem. Phys. **126**, 124507 (2007).
[53] K. J. Tielrooij, N. Garcia-Araez, M. Bonn, and H. J. Bakker, Science **328**, 1006 (2010).
[54] D. M. Mittleman, M. C. Nuss, and V. L. Colvin, Chem. Phys. Lett. **275**, 332 (1997).
[55] W. Wachter, Ph.D. thesis, Universität Regensburg, 2008.
[56] F. Kremer and A. Schönhals, *Broadband Dielectric Spectroscopy* (Springer, 2002).
[57] D. P. Fernandez, A. R. H. Goodwin, E. W. Lemmon, J. M. H. L. Sengers, and R. C. A. Williams, J. Phys. Chem. Ref. Data **26**, 1125 (1997).
[58] A. Luzar and J. Stefan, J. Mol. Liq. **46**, 221 (1990).
[59] J. G. Kirkwood, J. Chem. Phys. **7**, 911 (1939).
[60] M. Sharma, R. Resta, and R. Car, Phys. Rev. Lett. **98**, 247401 (2007).
[61] S. Senapati and A. Chandra, J. Phys. Chem. B **105**, 5106 (2001).
[62] J. Barthel, R. Buchner, K. Bachhuber, H. Hetzenauer, M. Kleebauer, and H. Ortmaier, Pure Appl. Chem. **62**, 2287 (1990).
[63] B. Maribo-Mogensen, G. M. Kontogeorgis, and K. Thomsen, J. Phys. Chem. B **117**, 10523 (2013).
[64] C. Cametti, F. De Luca, and A. Parmentier, J. Chem. Phys. **137**, 094908 (2012).
[65] We report the uncertainties as obtained from the least-squares fit; these values are unrealistically small and should be regarded as lower limits for the actual uncertainties, because they do not take into account systematic errors in the experiments.
[66] Based on the geometry of the reverse micelles (assuming a shape-independent hydration layer with thickness d) we expect a very small difference between the core water fraction S in spherical and cylindrical reverse micelles. In spherical reverse micelles $S_{\text{sphere}} = (r_{\text{sphere}} - d)^3/r_{\text{sphere}}^3$, and in cylindrical reverse micelles $S_{\text{cyl.}} = (r_{\text{cyl.}} - d)^2/r_{\text{cyl.}}^2$, where r is in both cases the radius of the reverse micelle. For $w_0 = 5$, we have $r_{\text{sphere}} = 1.05$, $d = 0.24$, and $r_{\text{cyl.}} \approx 2/3 \cdot r_{\text{cyl.}}$, so that $S_{\text{sphere}}/S_{\text{cyl.}} \approx 1.06$.
[67] H. J. Bakker, "Effective medium theory using the Onsager local field" (unpublished).